ARTICLE TYPE

Stretching the phenazine MO in dppz: The effect of phenyl and phenyl-ethynyl groups on the photophysics of Re(I) dppz complexes[†]

Holly van der Salm,[a,b] **Christopher B. Larsen,**[a,b] **James R. W. McLay,**[a] **Michael G. Fraser,**[a] **Nigel T. Lucas,**[a,b] **and Keith C. Gordon**[*a,b]

A series of dipyrido[3,2-a:2',3'-c]phenazine (dppz)-based ligands have been synthesised in which phenyl or phenyl-ethynyl linkers are terminated by ^{t}Bu or CN units. The corresponding [ReCl(CO)$_3$(L)] complexes are also prepared. Electrochemistry shows the ligand which contains a phenyl-ethynyl linker and CN substituent is most easily reduced (by 15 mV relative to the other ligands). All complexes are reduced and oxidised at similar potentials. Electronic absorption spectra are consistent with stabilisation of the LUMO by the binding of the metal centre, as complex spectra are red-shifted relative to their ligand. In addition, those containing phenyl-ethynyl linkers show spectra red-shifted (by 650 cm^{-1}) relative to their phenyl-linked analogues. Raman and resonance Raman spectroscopy combined with DFT and TD-DFT calculations are consistent with ligands showing π, π^* transitions, and complexes showing metal-to-ligand charge-transfer (MLCT) transitions as the lowest energy absorption. Ligands emit from the π, π^* excited state (λ_{em} ranging from 450 to 470 nm in CH$_2$Cl$_2$). The complexes show emission from both π, π^* and MLCT states; the λ_{em}(MLCT) lies at 650-666 nm. Transient lifetimes in CH$_2$Cl$_2$ are decreased by the CN substituent, as this increases k$_{nr}$. Transient resonance Raman spectra (TR^2) of ligands show spectral features associated with the LC state, and the strong similarities between these and complex spectra support an LC excited state at 355 nm for the complexes. Two-colour TR^3 spectra show only small differences to ground state spectra, the most obvious being a decrease in intensity of C≡C bands. For [ReCl(CO)$_3$(**2a**)] and [ReCl(CO)$_3$(**2b**)] an increase in intensity of a 1575 cm^{-1} band attributed to the dppz$^{\bullet-}$ species suggests that these complexes have significant MLCT state population between 20 – 60 ns after photoexcitation.

1 Introduction

Despite extensive study of dppz-based ligands and their metal complexes due to interesting photophysical properties, there has been relatively little focus on the effect of extending the conjugation of the ligand. Dppz has two low-energy unoccupied molecular orbitals which are close in energy but are spatially localised to different parts of the ligand - the phenanthroline MO on rings A, B and C and phenazine MO on rings B, D and E (see Fig. 1 and Fig. 2).[1–15] The phen MO has significant wavefunction amplitude at the chelating nitrogens, while the phz MO does not.

These two MOs are responsible for many of the photophysical properties of these compounds, in particular the 'light-switch' effect first observed by Friedman *et al.* in [Ru(bpy)$_2$(dppz)]$^{2+}$ in which the complex was emissive in
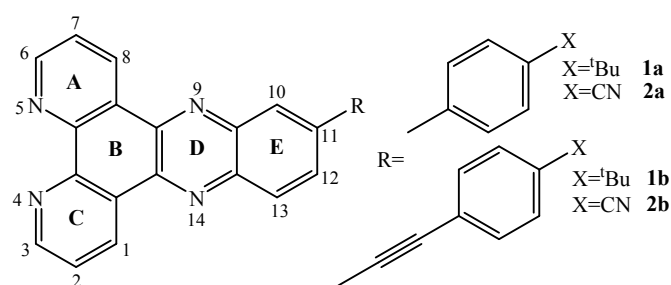
Fig. 1 Position numbering and ring labeling scheme for dppz, and structures of compounds studied.

(a) phenazine (phz) **(b)** phenanthroline (phen)
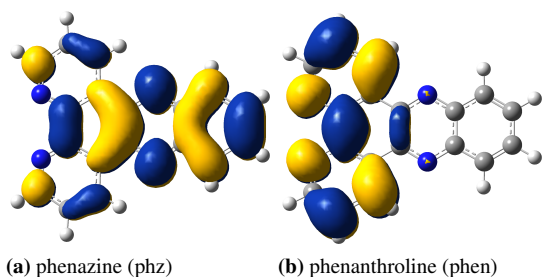
Fig. 2 Spatially segregated low energy unoccupied molecular orbitals.

aprotic solvents, but emission was quenched by protic solvents or by DNA.[16] This complex emits from a [3]MLCT state, which may be localised to either phen or phz (denoted MLCT(phen) and MLCT(phz) respectively), with MLCT(phen) an emissive state while MLCT(phz) is a non-emissive, or dark, state. It was initially thought that coordination of protic solvents or DNA to the phz nitrogens lowered the energy of MLCT(phz) while in aprotic solvents MLCT(phen) was lower in energy and hence emission was observed. This theory was modified by Brennaman *et al.*[17] based on variable temperature emission lifetimes, which indicated MLCT(phz) was always lower in energy for this compound, but a balance between enthalpic factors (favouring MLCT(phen)) and entropic factors (favouring MLCT(phz)) determined whether the compound was emissive or not.

Substituent effects can have a large influence on the electronic behaviour of dppz ligands and complexes. Kuhnt *et al.* studied substitution of dppz at the 2,7 or 11,12 positions with Br, phenyl, biphenyl and phenyl-ethynyl groups, as well as the [Ru(tbbpy)$_2$]$^{2+}$ complexes (where tbbpy = 4,4'-di-*tert*-butyl-2,2'-bipyridine) of these ligands.[12] Substitution of the phz part of dppz (i.e. 11,12 positions) with phenyl-ethynyl groups was found to break the C$_{2v}$ symmetry of the dppz ligand, as steric repulsion forced the phenyl groups to twist in opposite directions and distort ligand core planarity, with torsion angles of approximately 15° about the triple bond axis. Coordination of the metal only affects bond lengths of the phen part of the ligand, but it does induce coupling between vibrational modes. Aromatic substituents Ph, Ph-Ph and Ph-^{t}Bu at the 11 and 12 positions of dppz, and the [Ru(tbbpy)$_2$]$^{2+}$ complexes of these ligands were studied by Schafer *et al.*, with the aim of improving excited-state properties such as extending the lifetime.[18] This was successful, and complexes showed solvatochromic behaviour also.

Bilakhiya *et al.* extended dppz conjugation by linking two dppz ligands together, to act as a bridge between two metals. However, these showed poor electronic communication due to twisting about the bond linking the dppzs, proposed to reduce

conjugation, but with E_{red1} values much more positive than that of [ReCl(CO)$_3$(dppz)] or [Ru(bpy)$_2$(dppz)]$^{2+}$ and of the complexes studied here (-0.70 to -0.80 V, -1.42 [19]/-1.02 V[1] and -0.90 V, respectively) showed extended conjugation. E_{red2} lies at approximately -0.90 V, and both E_{red1} and E_{red2} are assigned as phz one-electron reductions.

In this study, we present dppz ligands substituted with either a Ph group or C≡C-Ph, thus altering the conjugation length; the phenyl group is further substituted with an electron-withdrawing (CN) or electron-donating (^{t}Bu) group which is expected to modulate MO energies (see Fig. 1). The *fac*-{ReCl(CO)$_3$} complexes of all ligands are also reported. In general, the compounds studied here showed behaviour consistent with what would be expected for dppz-type ligands with extended conjugation: more positive reduction potentials (E_{red}) than dppz, red-shifted electronic absorption spectra, TD-DFT and resonance Raman spectra showing lowest-energy transitions which are MLCT in nature for complexes, and other π,π^* transitions for ligands and complexes.

2 Experimental

2.1 Materials

Commercially available reagents were used as received. 11-bromodipyrido[3,2-a:2',3'-c]phenazine was prepared through literature methods.[20]

2.1.1 Suzuki-Miyaura Couplings. A mixture of 11-bromodipyrido[3,2-a:2',3'-c]phenazine (∼1.4 mmol), K$_2$CO$_3$ (∼7.0 mmol) and the corresponding boronic acid (∼2.1 mmol) in toluene (20 mL), water (10 mL) and EtOH (5 mL) was bubbled with argon for 15 min. Dichloro[1,1'-bis(diphenylphosphino)ferrocene] palladium(II) (∼0.07 mmol) was added and the mixture heated at reflux under an argon atmosphere overnight. The mixture was allowed to cool, and the volatiles were removed under reduced pressure. The crude product was purified by preparative column chromatography (basic Al$_2$O$_3$, CHCl$_3$) to afford the title compound.

2.1.2 11-(4-*tert*-butylphenyl)dipyrido[3,2-a:2',3'-c]phenazine (1a). The title compound (0.487 g, 83%) was obtained as a yellow solid. HRMS (ESI) calcd. for C$_{28}$H$_{23}$N$_4$ ([M + H]$^+$): m/z = 415.192. Found: m/z = 415.189. Anal. calcd. for C$_{28}$H$_{22}$N$_4$•H$_2$O: C, 77.75; H, 5.59; N, 12.95. Found: C, 77.92; H, 5.60; N, 12.94.

2.1.3 11-(4-cyanophenyl)dipyrido[3,2-a:2',3'-c]phenazine (2a). The title compound (0.421 g, 76%) was obtained as a yellow solid. HRMS (ESI) calcd. for C$_{25}$H$_{13}$N$_5$Na ([M + Na]$^+$): m/z = 406.106. Found: m/z = 406.108. Anal. calcd. for C$_{25}$H$_{13}$N$_5$•0.5H$_2$O: C, 76.52; H, 3.60; N, 17.85. Found: C, 76.86; H, 3.39; N, 17.74.

2.1.4 Sonogashira-Hagihara Couplings. A mixture of 11-bromodipyrido[3,2-a:2',3'-c]phenazine (∼1.3 mmol) and the corresponding acetylene (∼1.5 mmol) in NEt$_3$ (20 mL) was bubbled with argon for 15 min. CuI (∼0.1 mmol) and dichloro[1,1'-bis(diphenylphosphino)ferrocene] palladium(II) (∼0.05 mmol) were added and the mixture heated at reflux overnight. The mixture was allowed to cool, and the volatiles removed under reduced pressure. The crude product was purified by preparative column chromatography (basic Al$_2$O$_3$, CHCl$_3$) to afford the title compound.

2.1.5 11-((4-*tert*-butylphenyl)ethynyl)dipyrido[3,2-a:2',3'-c]phenazine (1b). The title compound (0.317 g, 57%) was obtained as a yellow solid. HRMS (ESI) calcd. for C$_{30}$H$_{22}$N$_4$Na ([M + Na]$^+$): m/z = 461.174. Found: m/z = 461.165. Anal. calcd. for C$_{30}$H$_{22}$N$_4$•0.9CHCl$_3$: C, 67.98; H, 4.23; N, 10.26. Found: C, 68.05; H, 4.27; N, 9.86.

2.1.6 11-((4-cyanophenyl)ethynyl)dipyrido[3,2-a:2',3'-c]phenazine (2b). The title compound (0.201 g, 36%) was obtained as a yellow solid. HRMS (ESI) calcd. for C$_{27}$H$_{13}$N$_5$Na ([M + Na]$^+$): m/z = 430.106. Found: m/z = 430.108. Anal. calcd. for C$_{27}$H$_{13}$N$_5$•H$_2$O: C, 76.22; H, 3.55; N, 16.46. Found: C, 76.38; H, 3.33; N, 16.67.

2.1.7 Rhenium Complexation. A mixture of ReCl(CO)$_5$ (∼0.3 mmol) and the corresponding dipyridophenazine (∼0.3 mmol) in EtOH (200 mL) was refluxed overnight. The mixture was allowed to cool and the residue purified by flash chromatography (basic Al$_2$O$_3$, CHCl$_3$) to afford the title compound.

2.1.8 *fac*-Chlorotricarbonyl(11-(4-*tert*-butylphenyl)dipyrido[3,2-a:2',3'-c]phenazine)rhenium(I). The title compound (0.171 g, 90%) was obtained as an orange solid. HRMS (ESI) calcd. for C$_{31}$H$_{22}$N$_4$O$_3$Re ([M-Cl]$^+$): m/z = 685.125. Found: m/z = 685.118. Anal. calcd. for C$_{31}$H$_{22}$ClN$_4$O$_3$Re: C, 51.70; H, 3.08; N, 7.78. Found: C, 51.76; H, 3.21; N, 7.83.

2.1.9 *fac*-Chlorotricarbonyl(11-(4-cyanophenyl)dipyrido[3,2-a:2',3'-c]phenazine)rhenium(I). The title compound (0.125 g, 69%) was obtained as an orange solid. HRMS (ESI) calcd. for C$_{28}$H$_{13}$N$_5$O$_3$Re ([M-Cl]$^+$): m/z = 654.057. Found: m/z = 654.059. Anal. calcd. for C$_{28}$H$_{13}$ClN$_5$O$_3$Re•2H$_2$O: C, 46.38; H, 2.36; N, 9.66. Found: C, 46.04; H, 1.96; N, 9.33.

2.1.10 *fac*-Chlorotricarbonyl(11-((4-*tert*-butylphenyl)ethynyl)dipyrido[3,2-a:2',3'-c]phenazine)rhenium(I). The title compound (0.170 g, 87%) was obtained as an orange solid. HRMS (ESI) calcd. for C$_{33}$H$_{22}$N$_4$O$_3$Re ([M-Cl]$^+$): m/z = 709.125. Found: m/z = 709.120. Anal. calcd. for C$_{33}$H$_{22}$ClN$_4$O$_3$Re•H$_2$O: C, 52.00; H, 3.17; N, 7.35. Found: C, 51.62; H, 2.96; N, 7.69.

2.1.11 *fac*-Chlorotricarbonyl(11-((4-cyanophenyl)ethynyl)dipyrido[3,2-a:2',3'-c]phenazine)rhenium(I). The title compound (0.150 g, 80%) was obtained as a yellow solid. HRMS (ESI) calcd. for C$_{30}$H$_{13}$N$_5$O$_3$Re ([M-Cl]$^+$): m/z = 678.057. Found: m/z = 678.062. Anal. calcd. for C$_{30}$H$_{13}$ClN$_5$O$_3$Re: C, 50.53; H, 1.84; N, 9.82. Found: C, 50.24; H, 1.95; N, 9.94.

2.2 Physical Measurements

Aldrich spectroscopic grade solvents were used for all spectroscopic measurements. Spectral data were analysed using GRAMS/32 AI (Galactic Industries) software.

2.2.1 NMR spectroscopy^{1}H NMR spectra were recorded at either 400 MHz on a Varian 400MR spectrometer or at 500 MHz on a Varian 500AR spectrometer. ^{13}C NMR Spectra were recorded at 126 MHz on a Varian 500AR spectrometer. All samples were recorded at 25°C. Chemical shifts were referenced internally to residual non-perdeuterated solvent using δ values as reported by Gottlieb et al.[21]

2.2.2 Mass spectrometry Electrospray ionization high resolution mass spectra were recorded on a Bruker MicroTOF-Q mass spectrometer operating in positive mode.

2.2.3 Elemental analysis Analysis of elemental composition was made by the Campbell Microanalytical Laboratory at the University of Otago, Dunedin, New Zealand, using a Carlo Erba 1108 CHNS combustion analyzer. The estimated error in the measurements is ±0.4%.

2.2.4 X-ray crystallography For X-ray crystallography, crystals were attached with Paratone N to a fiber loop supported in a copper mounting pin, and then quenched in a cold nitrogen stream. Data were collected at 100 (2) K using Cu Kα radiation (SuperNova, mirror monochromated) using a SuperNova, Dual, Cu at zero diffractometer with an Atlas detector. Data processing was undertaken with CrysAlisPro. A multiscan absorption correction was applied to the data. The structure was solved by direct methods with SHELXS-97, and extended and refined with SHELXL-97. The non-hydrogen atoms in the asymmetric unit were modeled with anisotropic displacement parameters and a riding atom model with group displacement parameters used for the hydrogen atoms. X-ray crystallographic data of **1a** is available in CIF format (Supporting Information). CCDC contains the supplementary crystallographic data for this article. These data can be obtained free of charge from The Cambridge Crystallographic Data Centre via www.ccdc.cam.ac.uk/data_request/cif.

Crystal data for **1a**•CHCl$_3$ follow: C$_{29}$H$_{23}$Cl$_3$N$_4$, M = 533.88, yellow needle, 1.04 × 0.05 × 0.04 mm^3, triclinic, a = 5.9069 (2) , b = 10.5275 (4) , c = 20.8395 (10) , α = 84.746 (4)°, β = 82.237 (3)°, γ = 76.627 (9)°, V = 1251.96 (9)^3, space

group P$\bar{1}$ (No. 2), Z = 2, μ(Cu Kα) = 3.520 mm^{-1}, 2θ_{max} = 148.24°, 8447 reflections measured, 4900 independent reflections (R_{int} = 0.0262). The final R1(F) = 0.0403 (I > 2σ(I)); 0.0470 (all data). The final wR2(F^2) = 0.1089 (I > 2σ(I)); 0.1145 (all data). GOF = 1.036. CCDC 1001500.

2.2.5 Absorption spectroscopy Absorption spectra were measured as dichloromethane solutions on a JASCO V550 UV-vis spectrometer.

2.2.6 Electrochemistry The electrochemical cell for cyclic voltammetry was made up of a 1 mm diameter platinum rod working electrode embedded in a KeL-F cylinder with a platinum auxiliary electrode and a Ag/AgCl reference electrode. The potential of the cell was controlled by an EG&G PAR 273 A potentiostat with model 270 software. Solutions were typically 10^{-3} M in CH$_2$Cl$_2$ with 0.1 M tetrabutylammonium hexafluorophosphate (Bu$_4$NPF$_6$) as supporting electrolyte, and were purged with nitrogen for approximately 5 min prior to measurement. The scanning speed was 0.1 V s^{-1}, and the cyclic voltammograms were calibrated against the decamethylferrocenium/decamethylferrocene (DMFc$^+$/DMFc) couple (-0.012 V in CH$_2$Cl$_2$) and are reported relative to the saturated calomel electrode (SCE) for comparison with other data by subtracting 0.045 V.

2.2.7 Raman spectroscopy FT-Raman spectra were collected on powder samples using a Bruker IFS-55 interferometer with a FRA/106S attachment. The excitation source was a Nd:YAG laser with an excitation wavelength of 1064 nm. Raman photons were detected with a liquid nitrogen-cooled D418T germanium diode. Spectra were measured with 196 scans, with laser power of 50 mW and spectral resolution of 4 cm^{-1}. Resonance Raman spectra were recorded using a previously described setup.[22–25] Excitation wavelengths 351, 406 and 413 nm were provided by a krypton ion laser (Coherent Inc.); 448 nm was provided by a crystal diode laser (Crysta-Laser). Concentrations were typically 1 mM in CH$_2$Cl$_2$.

Transient resonance Raman spectra were recorded at room temperature on CH$_2$Cl$_2$ solutions with typically 1 mM concentration. Scattered photons were focused on an Acton SpectraPro 2500i 0.5 m spectrograph and dispersed by a 1200 grooves / mm grating onto a PI-MAX intensified camera (Princeton Instruments). Samples were pumped and probed at either 355 nm or 532 nm using pulsed third-harmonic or second-harmonic radiation at 10 Hz from a Brilliant Nd:YAG (Quantel) laser, with a pulse width of approximately 6 ns. Laser radiation was rejected prior to the spectrograph using long-pass filters (Semrock Inc.) Both lasers were used for two-colour pump-probe experiments, for which Q-switch and flashlamp timing was controlled using a DG535 four-channel digital delay pulse generator (Stanford Research Systems Inc.). For two-colour experiments, pulse power was 1.60

mJ for 355 nm and 0.8 mJ for 532 nm. The CCD controller was triggered from the Q-switch signal of the probe laser. The laser spot size and pump-probe beam overlap were determined from burn profiles.

2.2.8 Transient absorption Transient absorption spectra were recorded on CH$_2$Cl$_2$ solutions with concentration typically 1×10^{-5} M which were degassed under argon for 10 minutes prior to measurement. Transients were acquired using a LP920K TA system (Edinburgh Instruments) with 1 Hz radiation from 355 nm pulsed Nd:YAG laser used for transient Raman spectra.
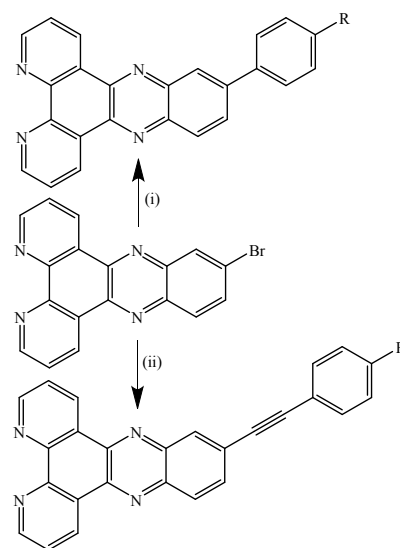
Fig. 3 Ligand synthesis. (i) 4-*tert*-butylphenylboronic acid or 4-cyanophenylboronic acid, K$_2$CO$_3$, PdCl$_2$(dppf), toluene, water, EtOH, reflux; (ii) 4-tert-butylphenylacetylene or 4-cyanophenylacetylene, CuI, PdCl$_2$(dppf), NEt$_3$

2.3 Computational methods

Density functional theory using the Gaussian09 program suite[26] was used for calculations on these compounds. A B3LYP functional was employed for *in vacuo* optimisations and calculations of vibrational frequencies. Electronic transitions were predicted using time-dependent DFT (TD-DFT) both *in vacuo* and using the IEFPCM (integral equation formalism polarisable continuum model) solvent model[27,28] with dichloromethane, using the B3LYP and CAM-B3LYP functionals. Mulliken charge analysis was carried out from calculations that included the solvent model and utilised the B3LYP functional. Emission wavelengths were calculated by optimising the lowest energy triplet state, then carrying out a single point energy calculation on the singlet state with this geometry, and finding the energy difference.[29] In all calculations,

the LANL2DZ effective core potential was used to model rhenium atoms, as this has been shown to be suitable in many related systems, while the remaining atoms were modelled using a 6-31G(d) basis set. Calculated vibrational energies (cm^{-1}) were scaled as to minimise the mean absolute deviation between experimental and calculated values; scale factors were 0.975.[10,15,30–32] Calculated Raman activities (S_j) were converted to Raman intensities at 1064 nm. Molecular orbitals were visualised using Gaussview (Gaussian Inc.) and vibrational modes were illustrated using Molden.[33]

3 Results and discussion

3.1 Synthesis and Structure

The synthesis of the dppz ligands was achieved through Suzuki-Miyaura (**1a** and **1b**) and Sonogashira-Hagihara (**2a** and **2b**) cross-couplings with 11-bromodipyrido[3,2-a:2',3'-c]phenazine (Fig. 3). Whilst Suzuki couplings on dppz have been previously studied,[18,34] this study represents the first attempt at directly functionalizing dppz through other cross-coupling reactions. [ReCl(CO)$_3$(dppz)] complexes were prepared utilizing literature methods for related complexes.

An X-ray crystal structure of **1a** was obtained (Fig. 4), using a crystal grown through diffusion of hexane into a CHCl$_3$ solution. **1a** crystallised in the triclinic P-1 space group. In this structure, the dppz skeleton is slightly twisted, with rings A and C (see Fig. 1) twisted at an angle of 6.37° from rings D and E. The phenyl group is rotated from ring E, with a torsion angle of 32.20°. Each molecule of **1a** co-crystallises with one molecule of CHCl$_3$, the acidic proton of which hydrogen-bonds with the phen-based nitrogens (N1 and N2) in a bifurcated manner. A comparison between the crystal structure (see Fig. 4) and calculated *in vacuo* optimised structure of **1a** shows a mean deviation in bond length of 0.4%, while the phenyl ring of the substituent is twisted in opposite directions in the calculated structure and crystal structure, but the dihedral relative to dppz(phz) is found to be similar. This shows satisfactory agreement, and assists in validating that DFT calculations are representative of the behaviour of the real system.

In the absence of crystal structures, a comparison between experimental and calculated FT-Raman spectra allows validation of calculations, as in order to correctly predict vibrational mode position and intensity, the potential energy surface must be calculated correctly, and therefore electronic parameters may be considered reliable. The difference between calculated and experimental bands are parameterised by the mean absolute deviation (MAD) in wavenumber for the most intense bands. For the compounds studied here, MAD values ranged from 4.4 to 10.0 cm^{-1}, and calculated spectra were scaled by 0.975.
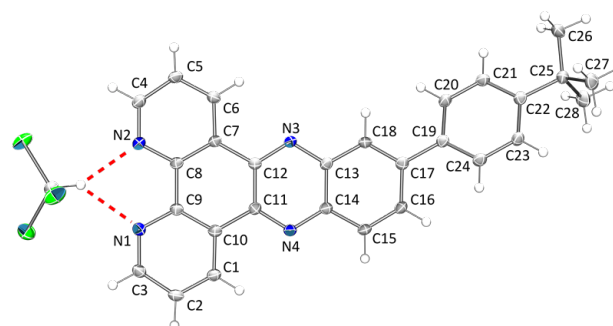
Fig. 4 Crystal structure of **1a** with 50% displacement ellipsoids, co-crystallised with one molecule of CHCl$_3$.

3.2 Electrochemistry

Table 1 Electrochemical data for compounds studied. E_{red} and E_{ox} are recorded in CH$_2$Cl$_2$ against DMFc$^+$/DMFc with supporting electrolyte 0.1 M Bu$_4$NPF$_6$ and reference electrode Ag/AgCl. Values are converted to SCE with -0.045 V. ΔE_{red} refers to the difference between a complex and its respective ligand.

Ligand	E_{red}/V	Complex	E_{red} / V	E_{ox} / V	ΔE_{red} / V
dppz	-1.28	[ReCl(CO)$_3$(dppz)]	-1.01		0.27
dppz-Me	-1.30	[ReCl(CO)$_3$(dppz-Me)]	-1.04		0.26
dppz-CN	-0.91	[ReCl(CO)$_3$(dppz-CN)]	-0.63		0.28
dppz-CO$_2$Et	-1.12	[ReCl(CO)$_3$(dppz-CO$_2$Et)]	-0.86		0.26
dppz-Br	-1.16	[ReCl(CO)$_3$(dppz-Br)]	-0.92		0.24
1a	-1.22	[ReCl(CO)$_3$(**1a**)]	-0.96	1.45	0.26
2a	-1.21	[ReCl(CO)$_3$(**2a**)]	-0.90	1.45	0.31
1b	-1.22	[ReCl(CO)$_3$(**1b**)]	-0.90	1.46	0.32
2b	-1.07	[ReCl(CO)$_3$(**2b**)]	-0.90	1.46	0.17

The electrochemical data for the ligands and complexes, and some related systems, are presented in Table 1. These electrochemical data allow an insight into the relative energies of electron accepting (LUMO) and donating (HOMO) molecular orbitals. The effect of substituents on the redox properties of dppz ligands and their complexes has been well studied. The data show that the phenyl substituent has only a minor stabilising effect on the E_{red}. The reduction generally occurs at the phz MO and the lack of direct conjugation, as indicated in the structural, experimental and calculated data, between the dppz framework and the substituent is consistent with the modest stabilisation of the reduction potential. Interestingly, the ethynyl linkage, in which conjugation across the entire ligand is possible, does not have a dramatic effect on E_{red}. For this system (**1b**) the effect is negligible, and for **2b** which has an electron-withdrawing CN group a stabilisation of ∼150 mV is observed. Direct substitution of CN at the phz E ring results in a much larger shift in E_{red} (+370 mV)

relative to dppz.[10] For comparison, the electron donating substituent in dppz-Me has a minor destabilising effect (20 mV[35]) while electron withdrawing substituents such as COOEt, Br and NO$_2$ are stabilising to varying degrees (160[32], 120[32] and 230 mV,[35] respectively). These compounds are all stabilised by ∼260 mV by Re(I) complexation; this value is more varied for the complexes studied herein.

3.3 Vibrational Spectroscopy

The Raman spectra for the ligands and complexes show spectral similarities to other dppz systems.[5,12,15,20,30,36,37] Spectra are dominated by a phenazine mode around 1400 cm^{-1}; this mode is assigned using DFT calculations[30], isotopomers[5] and substitution studies with various groups at phen and phz positions.[12,13] Another strong mode is observed at 1450 cm^{-1}, which here is shown by DFT calculations to be delocalised over the dppz ligand, similar to other dppz substituted at the phenazine;[12,30] for unsubstituted dppz this is a phen mode.[15] DFT calculations show the strong band around 1600 cm^{-1} to be a vibration of the substituent phenyl group; this is consistent with other compounds that have a phenyl substituent at the E-ring.[18,34] **1a**, **1b** and their complexes show a strong mode at 1110 cm^{-1} which is assigned as a Ph-^{t}Bu vibration using DFT calculations. Compounds which contain CN groups show a C≡N stretching mode around 2220 cm^{-1} (calc. 2280 cm^{-1}), and those with ethynyl substituents show C≡C stretching around 2200 cm^{-1} (calc. 2240 cm^{-1}) which is very strong in non-resonant spectra as the C≡C bond is highly polarisable. Correlation between experimental spectra and calculated spectra is good, as shown in Fig. 5, and MAD values are sufficiently small to show DFT calculations model the system in an acceptable way, hence vibrational assignments are likely to be reliable. In addition, assignments made by DFT are consistent with literature where available.

3.4 Electronic Absorption Spectra, TD-DFT calculations and resonance Raman spectroscopy

Electronic absorption spectra are shown in Fig. 6 and electronic absorption and emission data with the summary of calculated data are presented in Table 2. These spectra resemble those of many other substituted dppz ligands[38] and their Re(I) complexes. Ligands **2a** (395, 377 nm) and **2b** (407, 387 nm) show spectra which resemble dppz (379, 367 nm[30]), dppz-Me (385, 366 nm[39]) and dppz-COOH (386, 366 nm[39]), although red-shifted in a similar manner to dppz−(SCN)$_2$(401, 381 nm[30]). The lower energy band is assigned as n→ π*, and the higher energy band as π → π*; other bands at even higher energy are also π → π*. For **1a** and **1b** these bands are less defined, although the asymmetry in the shape of the lowest energy absorption band suggests both contribute to this ab-
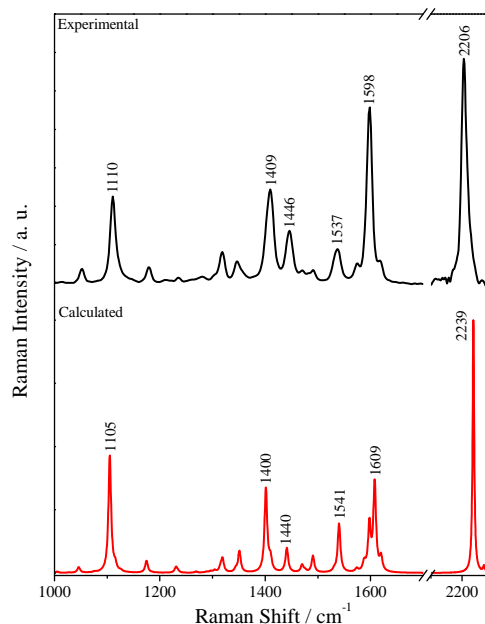
Fig. 5 Experimental FT-Raman and DFT calculated Raman spectra of [ReCl(CO)$_3$(**2b**)].

sorption manifold. For **2a** and **2b**, complexation results in the appearance of the tailing MLCT band. This is consistent with literature, as Re complexation stabilises the phz MO, decreasing the LUMO energy.[3,7,9,14,35,40] Ethynyl-linked compounds (**1b** and **2b**) show absorption bands at lower energy than their phenyl-linked counterparts, as extending the dppz conjugation also lowers the energy of the phz MO. The nature of electronic transitions can be probed using TD-DFT calculations and resonance Raman spectroscopy.

Table 2 Summary of electronic absorption (experimental and calculated), band assignments and emission wavelengths for ligands and complexes (CH$_2$Cl$_2$, room temp.). Detailed TDDFT data is presented in Table S1

Compound	Expt. λ / nm (ε / 10^4 M^{-1} cm^{-1})	Calc. λ / nm (f)	Assign.	λ_{em} / nm
1a	402 (1.9)	405 (0.4)	π, π*	
2a	395 (2.6)	385 (0.3)	π, π*	
1b	412 (2.1)	441 (0.75)	π, π*	
2b	406 (2.9)	417 (0.99)	π, π*	
[ReCl(CO)$_3$(**1a**)]	412 (2.3)	424 (0.3)	MLCT	698
	396 (2.1)	333 (0.8)	π, π*	490
[ReCl(CO)$_3$(**2a**)]	401 (1.8)	390 (0.25)	MLCT	665
	384 (1.9)	-	π, π*	498
[ReCl(CO)$_3$(**1b**)]	424 (1.9)	472 (0.7)	MLCT	621
	396 (1.7)	-	π, π*	504
[ReCl(CO)$_3$(**2b**)]	411 (3.3)	471 (0.14)	MLCT	665
	396 (3.1)	431 (0.8)	π, π*	458

The resonance Raman spectra for the complexes show modulation of band intensities with excitation wavelength. The
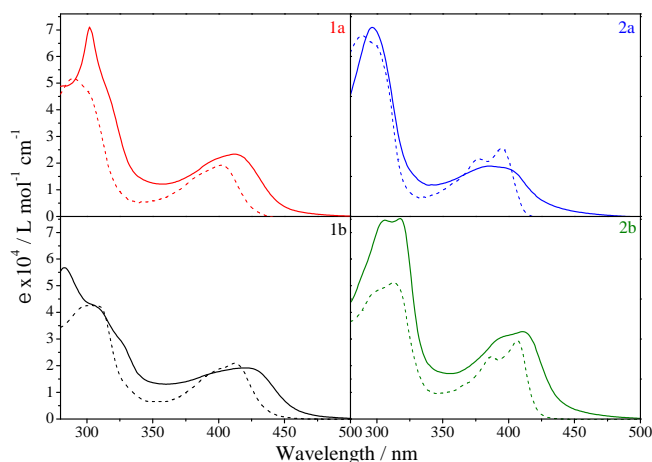
Fig. 6 Electronic absorption spectra of ligands (dashed lines) and complexes (solid lines) recorded in CH$_2$Cl$_2$ solution.

spectral data for [ReCl(CO)$_3$(**2b**)] is shown in Fig. 7 (for additional mode depictions see Figure S3). The λ_{ex} scan three distinct transitions, in the blue (λ_{ex} = 351 nm), strong band enhancements are observed at 1416 and 1542 cm^{-1}. In addition, bands at 2030 cm^{-1} and 2215 cm^{-1} are very weak, despite the latter having a strong normal Raman cross section. The bands at 1416 and 1542 cm^{-1} are assigned as phz modes (see Fig. 8). This is consistent with TD-DFT calculations that suggest the transition predicted at 318 nm and corresponding to the observed feature at 344 nm is π, π^* LC in nature, with electron density changes at the phen and phz moieties (+33, -3 respectively) and little density change at the donor unit. With 406 and 413 nm excitation, the relative intensity of the 1542 cm^{-1} is diminished and that of 1416 cm^{-1} increased. Furthermore, features at 1576, 1602 and 1625 cm^{-1} all gain intensity *and* the C≡C mode at 2215 cm^{-1} is enhanced. This is consistent with a transition that has considerable linker character. The band at ∼1602 cm^{-1} is assigned to a substituent phenyl mode and its enhancement also supports substituent character for transitions at these wavelengths. On going further to the red (λ_{ex} = 448 nm) the enhancement of the phenyl mode is retained although the intensity of the C≡C mode drops, additionally the 2030 cm^{-1} CO mode is observed. The presence of the CO mode is consistent with an MLCT transition but the differences in enhancement of the linker modes points to a change in the electronic transition to the red.

Other studies on dppz compounds show similarities in band enhancements, consistent with the assignment of a ligand-centered π, π^* state around 300 nm, and MLCT transitions at longer wavelengths for metal complexes. Many show the enhancement of 1400-1420 cm^{-1} and 1540-1550 cm^{-1} phz modes at wavelengths in the UV, consistent with population of the phz-based LUMO in a π, π^* transition.[2,20,30,32,34] Mov-
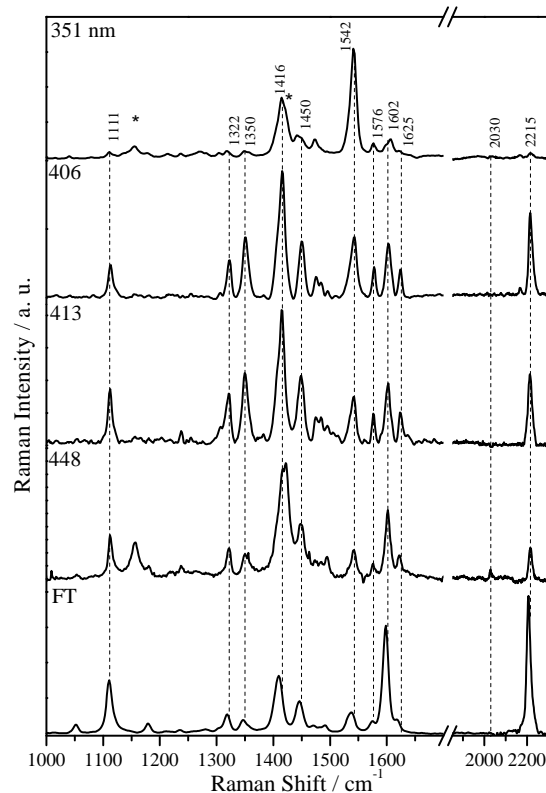
Fig. 7 Resonance Raman spectra of [ReCl(CO)$_3$(**2b**)] at several excitation wavelengths recorded in DCM with approximately 1 mM concentration. FT-Raman spectrum was recorded on a solid sample. Solvent bands are denoted *.

ing to longer wavelengths shows dimunition of these bands and enhancement of the CO 2030 cm^{-1} mode associated with an MLCT transition. For the ligands dppz−PhNPh$_2$ and dppz−PhNMe$_2$, the lowest energy band is intra-ligand charge transfer (ILCT) from the amine to dppz, and shows enhancement of a 1600 cm^{-1} mode which is vibration of the phenyl group linking the phz part of dppz to the nitrogen; enhancement of this mode is associated with involvement of the linker.[34]

3.5 Emission

The ligands and complexes show emission in solution phase. The emission spectra of the ligands show a Stokes shift of approximately 2000 cm^{-1}; the emissive state is assigned as π, π^* in nature. Consistent with this, the emission spectra do not shift with solvent. Solvatochromic behaviour has been observed in dppz-type ligands in which the emission has charge-transfer character.[34] For the complexes the data are less clear cut. Each complex shows two emission bands in room temperature solution, see Fig. 9. The higher energy of these bands corresponds to the ligand emission, but for three of the complexes ([ReCl(CO)$_3$(**1b**)], [ReCl(CO)$_3$(**2a**)] and [ReCl(CO)$_3$(**2b**)]) there is a red emission around 670 nm that is assigned as MLCT in nature. Changing the solvent causes shifting of this band along with a change in the relative intensities of the π, π^* and MLCT emission bands. In the case of [ReCl(CO)$_3$(**1a**)] there appears to be a very weak extended emission around 700 nm that would be consistent with an MLCT state. Analysis of solutions prior to and after emission studies indicate no photochemical degradation and the presence of complex only in the samples used.

3.6 Triplet state calculations

The calculation of the triplet state can provide insight into the nature of the lowest energy excited state in dppz.[37] Some care is required as the nature of excited states in dppz complexes can involve LC and MLCT states of differing nature (i.e. phen or phz-based, see Introduction). In order to better model the compounds of interest herein the calculations were performed in a solvent field with parameters for CH$_2$Cl$_2$. In all cases, frequency calculations were run to verify the absence of imaginary frequencies consistent with the occupation of a local energy minimum, and for all cases the lowest energy triplet state is found to be predicted to be MLCT in nature. The structural changes between the excited state and ground state manifest in two ways: firstly for the CN substituted systems (namely [ReCl(CO)$_3$(**2a**)] and [ReCl(CO)$_3$(**2b**)]) the CN bond length is increased (by 0.01 nm). Secondly the C≡C bond in systems which have this is also increased in the triplet state relative to the singlet state (by 0.17 nm). The triplet calculations

also offer a method of estimating the emission wavelength.[29] Experimental spectra and the calculated position of emission based on the energy gap show qualititave agreement, indicating MLCT emission should occur around 700 nm.

3.7 Transient absorption spectroscopy

All ligands showed μs lifetimes of the transient absorbing states, see Table 3, which are decreased in their respective complexes. [ReCl(CO)$_3$(**2a**)] and [ReCl(CO)$_3$(**2b**)] have lifetimes which are very short for this type of complex, indicating the CN group influences excited state decay pathways. It has previously been observed that CN decreases the lifetime of excited states due to the electron withdrawing nature affecting electron transfer[41] and then C≡N vibration acting as an electron acceptor similar to ν(CO).[42] The lifetimes of the emitting state are all shorter than the resolution of the instrument, and thus are less than 8 ns. Positive transient signals are observed around 350 nm and 450-650 nm, and bleaches are observed which correspond to ground state absorption bands, around 400 nm, see 10 and S5. Ligands and complexes show similar spectra, but features are quite broad. The feature centered around 550 nm may be associated with dppz$^{\bullet-}$,[1,3,10,43] but transient absorption cannot distinguish the nature of the excited state formed. Consequently, transient and time-resolved Raman studies were used to give a more definitive insight into the nature of this state.

Generally dppz ligands show μs lifetimes, and these are decreased by metal complexation, consistent with what is observed here.[10,20,34] Lifetimes can vary considerably with solvent and temperature, due to the environmental sensitivity of dppz,[8] and also depend on the nature of the probed state.[15] For example, Kuimova et al. measured a 10 μs lifetime for [Re(CO)$_3$(py)(dppz−(CO$_2$Et)$_2$)]$^+$ in MeCN, while Dyer et al. measured 3.5 μs for [Re(CO)$_3$(py)(dppz)]$^+$ in MeCN; in both cases this state is assigned as π, π^* in nature.

Table 3 Lifetimes fitted from transient absorption traces.

Compound	τ / ns
1a	2350 ± 370
1b	3730 ± 560
2a	3240 ± 510
2b	1390 ± 130
[ReCl(CO)$_3$(**1a**)]	620 ± 180
[ReCl(CO)$_3$(**1b**)]	650 ± 310
[ReCl(CO)$_3$(**2a**)]	30 ± 5
[ReCl(CO)$_3$(**2b**)]	90 ± 10

3.8 Transient resonance Raman spectroscopy

In single colour transient resonance Raman spectroscopy the thermally equilibrated excited (THEXI) state is

(**a**) 1416 cm^{-1} (**b**) 1542 cm^{-1} (**c**) 1603 cm^{-1} (**d**) 1624 cm^{-1}
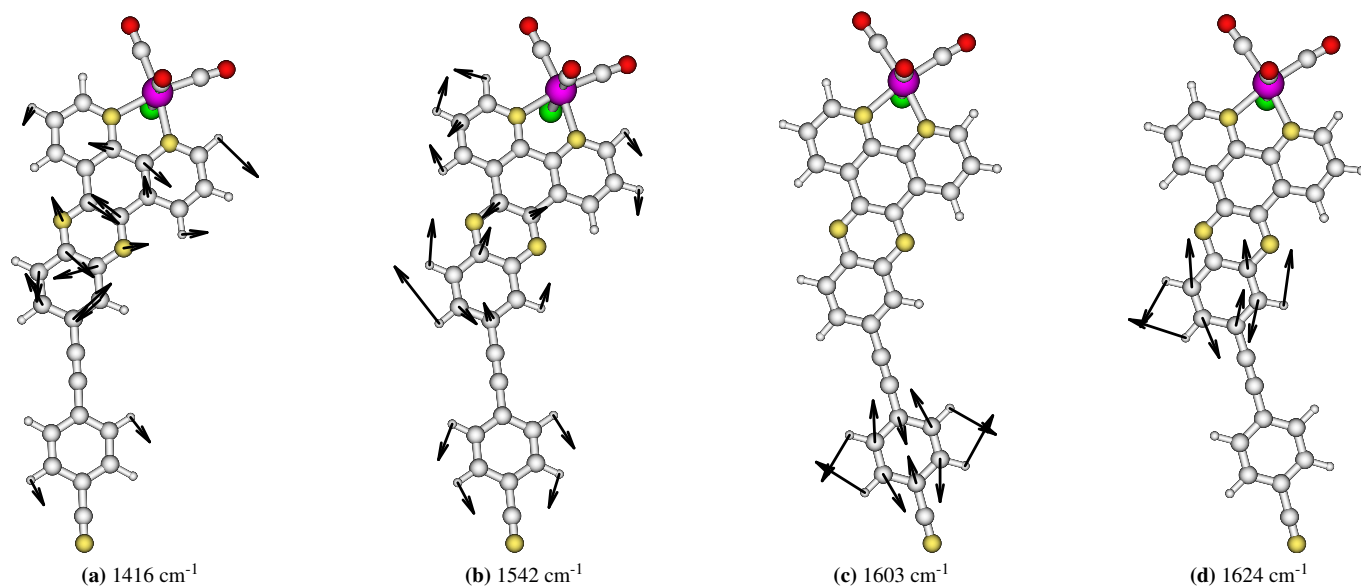
Fig. 8 Selected vibrational modes of [ReCl(CO)$_3$(**2b**)] enhanced in resonance Raman spectra of all complexes.
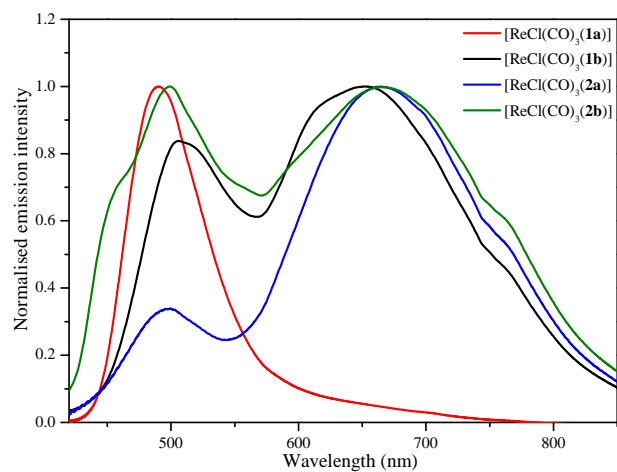
Fig. 9 Normalised emission spectra of complexes recorded in CH$_2$Cl$_2$.
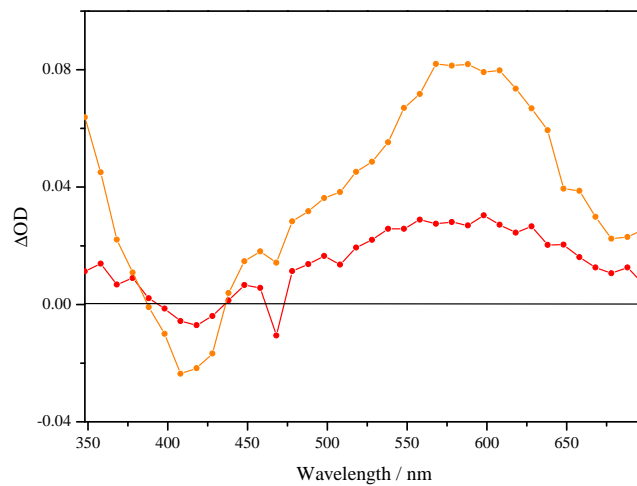
Fig. 10 Transient absorption spectra of **1a** (red) and [ReCl(CO)$_3$(**1a**)] (orange) obtained 40 ns after 355 nm excitation. Compounds are in deoxygenated CH$_2$Cl$_2$ solution with concentration of approximately 1×10^{-5} M.
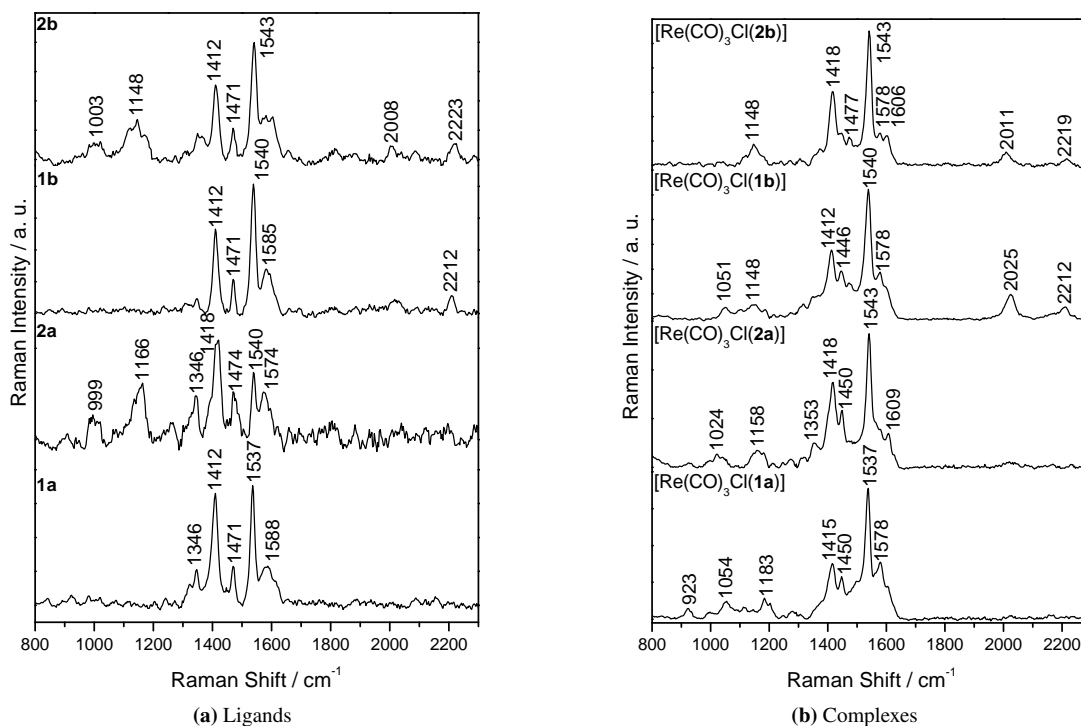
Fig. 11 Transient resonance Raman spectra (355 nm excitation) for CH_2Cl_2 solutions.

probed.[31,44–48] Two challenges exist in such experiments: firstly if the excited state τ is similar to that of the laser pulse then it is possible to observe scattering from both ground and excited states. The bands associated with the excited state may be discerned in this case by variable power studies as the excited state band intensities are a function of the square of laser power. Thus a log(intensity) vs log(power) plot will have a gradient > 1;[49] secondly the single colour experiment has no temporal control, that is the signal pertains to the excited state or *states* present in the irradiated volume during the laser pulse*. Thus short-lived states may contribute to the observed signal even though they do not persist >10 ns duration. This second issue is important because it limits how effective such an experiment can be in distinguishing between differing excited states with time; it is a time-average of the population. By comparing the single-colour TR^2 spectrum of the ligands with that of the complexes one can determine if the transient probed has similar electronic structure.[10] These data are shown in Fig. 11. Previous studies have identified

that spectral markers for the π,π^* state of $[Re(CO)_3Cl(dppz)]$ lie at 1270 cm^{-1}.[4,35,37] This is distinct from the main spectral feature of dppz$^{\bullet-}$ which is a marker band at 1581 cm^{-1}.[5] The single-colour data for the ligands provides the marker bands for the π,π^* states (Fig. 11). These show bands that are not shifted from the ground state. Such spectral behaviour is not uncommon in rigid ligand systems and is observed in 2,9-dimethyl-1,10-phenanthroline (dmp) and its radical anion. In that case, the spectra only show the loss of single band (at 1315 cm^{-1}) on going from the neutral ligand to radical anion (phen $\rightarrow$ phen$^{\bullet-}$) through population of an MLCT excited state.[50] It is noteworthy that the CN substituted ligands show strong transient bands at 1148 and 1003 cm^{-1} for **2b** and 1166 and 999 cm^{-1} for **2a**. The spectra of the corresponding complexes also show these bands, supporting a π,π^* assignment for the duration of the single pulse. The data for the ^{t}Bu substituents is less distinct but the spectra of the ligands and complexes appear similar so that a π,π^* assignment is not inconsistent with these data.

Fig. 12 shows spectra obtained from a two-colour experiment where solutions were pumped at 355 nm and probed with 532 nm; the delay between the pump and probe was either 20 ns or 65 ns - a longer delay gives better signal-to-noise ratio as less prompt emission is collected, but this is dependent on excited state lifetime, as if the delay time exceeds this (e.g.

---

* Concentrations ranged from 0.2 mM to 5 mM, depending on solubility; using the highest concentration, a laser spot size of 500 μm and assuming a penetration depth of 1 mm,[22] this gives $\sim6\times10^{14}$ molecules in an irradiated volume of $\sim2\times10^{-10}$ m^3. Reported spectra were recorded with a laser power of approximately 2 mJ per pulse, which equates to $\sim3.6\times10^{15}$ photons, which gives a photon/molecule ratio of at least 6, indicating it is likely all probed molecules are in the excited state.
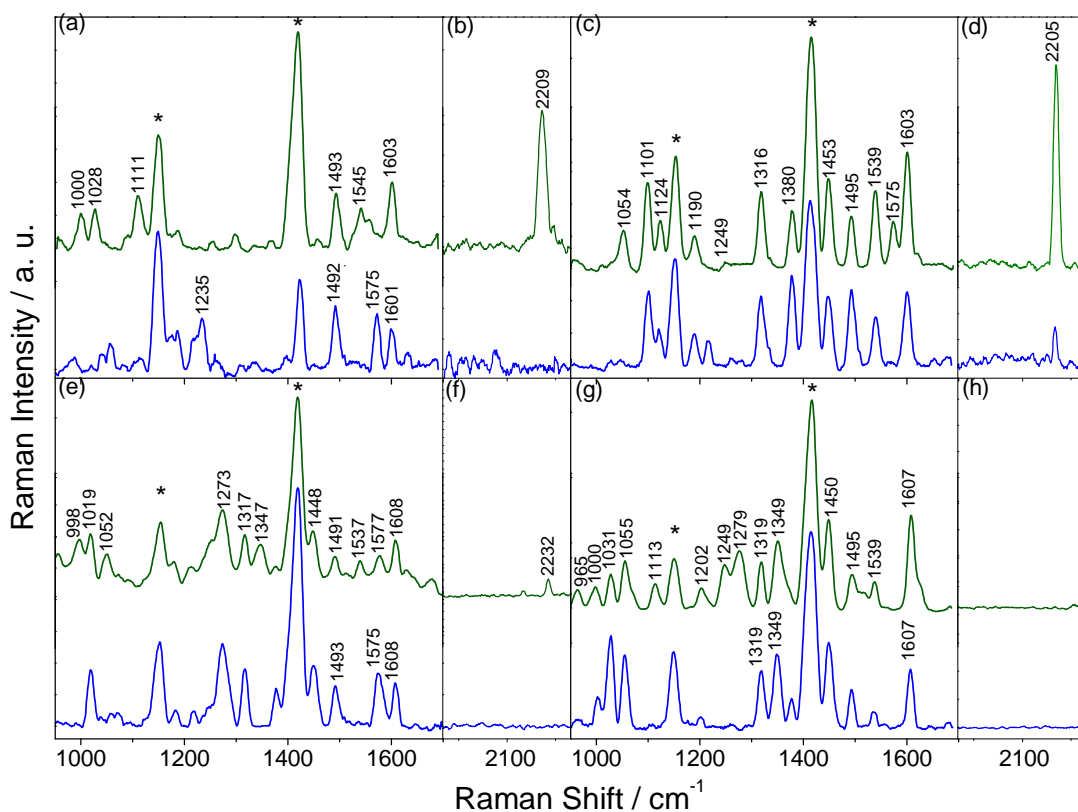
Fig. 12 Single colour TR^2 spectra (532 nm) (green traces) and two-colour spectra (355 nm pump, 532 nm probe) (blue traces) of [ReCl(CO)$_3$(**2b**)] (a) and (b); [ReCl(CO)$_3$(**1b**)] (c) and (d); [ReCl(CO)$_3$(**2a**)] (e) and (f) and [ReCl(CO)$_3$(**1a**)] (g) and (h). The time delay between pump and probe is 65 ns except for [ReCl(CO)$_3$(**2a**)], where the delay is 20 ns. Solvent bands are marked *. Spectra are smoothed with a 10-point adjacent-average and spectral windows are shown on the same intensity scale for a given compound.

[ReCl(CO)$_3$(**2a**)] has τ=30 ns) there will be no excited state to probe. Pump-probe spectra were compared to single-colour 532 nm TR^2 spectra. The CN substituted systems show similar TR^3 spectra; notably they show strong transient bands at 1603/9, 1575 and 1493/1 cm^{-1}. Furthermore the transient nature of the spectra is confirmed by the loss of ground state bands at 1545 cm^{-1} for [Re(CO)$_3$Cl(**2b**)] and 1537 cm^{-1} for [Re(CO)$_3$Cl(**2a**)]. These spectral features are consistent with an MLCT excited state.[5] The spectral changes are much less distinct for the ^{t}Bu systems. For [ReCl(CO)$_3$(**1b**)] a small feature is observed at 1249 cm^{-1} and ground state bands are depleted (at 2205 and 1575 cm^{-1}) for [ReCl(CO)$_3$(**1a**)] ground state bands at 1279 and 1249 cm^{-1} bands are depleted. The spectral features are not definitive in this case and may be either due to a π,π^* or MLCT state. These data are consistent with the emission spectra that show the presence of both π,π^* and MLCT emissive states in [ReCl(CO)$_3$(**2b**)], [ReCl(CO)$_3$(**2a**)] and [ReCl(CO)$_3$(**1b**)]. In the single colour experiments the temporal sampling of the excited state is 10 ns and thus the short-lived π,π^* is prevalent; however in the

two-colour experiment the temporal sampling is either 20 or 60 ns after excitation and this favours the longer-lived MLCT state.

4 Conclusions

The effect of extending the dppz framework with either phenyl or phenyl-ethynyl linkers, and ^{t}Bu or CN substituents on both ligands and [ReCl(CO)$_3$(L)] complexes has been investigated using a variety of experimental and computational techniques. Electrochemistry shows **2b** to be the most easily reduced, by 15 mV, while the other ligands are all very similar. Complexation stabilises the electrochemical LUMO, and all complexes show very similar E$_{red}$ and E$_{ox}$ values. Electronic absorption spectra show ligands containing the ethynyl linker to be red-shifted relative to their phenyl-linker analogue, while in all cases complexation causes a red-shift due to stabilisation of the acceptor MO. Raman, DFT calculations, resonance Raman and TD-DFT calculations are consistent with π,π^* states for ligands, where the phz MO in particular shows extensive

delocalisation across the linker and substituent. The lowest energy transitions for complexes are MLCT in nature. Ligands emit from LC states, while the emissive state of complexes appears to be solvent-dependent. The lifetime of the excited state measured in ns transient absorption spectra is reduced by CN substituent, as the CN vibrational mode is an energy acceptor. Transient resonance Raman spectra of the ligands act as models of the LC excited state, and 355 nm TR_2 spectra of the complexes are assigned to π, π^* states due to the similarity between these spectra. Two-colour pump-probe Raman spectra show a spectral changes including a decrease in intensity of C≡C bands in molecules that contain them, and the presence of the MLCT dppz$^{\bullet-}$ marker band in the CN substituted systems.

References

1 E. Amouyal, A. Homsi, J.-C. Chambron and J.-P. Sauvage, *Dalton Trans.*, 1990, 1841–1845.

2 J. R. Schoonover, W. D. Bates and T. J. Meyer, *Inorg. Chem.*, 1995, **34**, 6421–6422.

3 J. Fees, M. Ketterle, A. Klein, J. Fiedler and W. Kaim, *Dalton Trans.*, 1999, **15**, 2595–2600.

4 M. R. Waterland and K. C. Gordon, *J. Raman Spectrosc.*, 2000, **31**, 243–253.

5 B. J. Matthewson, A. Flood, M. I. J. Polson, C. Amstrong, D. L. Phillips and K. C. Gordon, *Bull. Chem. Soc. Jpn.*, 2002, **75**, 933–942.

6 J. Dyer, D. C. Grills, P. Matousek, A. W. Parker, M. Towrie, J. A. Weinstein and M. W. George, *Chem. Commun.*, 2002, 872–873.

7 M. K. Kuimova, W. Z. Alsindi, J. Dyer, D. C. Grills, O. S. Jina, P. Matousek, A. W. Parker, P. Portius, X. Z. Sun, M. Towrie, C. Wilson, J. Yang and M. W. George, *Dalton Trans.*, 2003, 3996–4006.

8 J. Dyer, C. M. Creely, J. C. Penedo, D. C. Grills, S. Hudson, P. Matousek, A. W. Parker, M. Towrie, J. M. Kelly and M. W. George, *Photochem. Photobiol. Sci.*, 2007, **6**, 741–748.

9 M. K. Kuimova, X. Z. Sun, P. Matousek, D. C. Grills, A. W. Parker, M. Towrie and M. W. George, *Photochem. Photobiol. Sci.*, 2007, **6**, 1158–1163.

10 N. J. Lundin, P. J. Walsh, S. L. Howell, A. G. Blackman and K. C. Gordon, *Chem. Eur. J.*, 2008, **14**, 11573–11583.

11 S. P. Foxon, M. A. H. Alamiry, M. G. Walker, A. J. H. M. Meijer, I. V. Sazanovich, J. A. Weinstein and J. A. Thomas, *J. Phys. Chem. A*, 2009, **113**, 12754–12762.

12 C. Kuhnt, S. Tschierlei, M. Karnahl, S. Rau, B. Dietzek, M. Schmitt and J. Popp, *J. Raman Spectrosc.*, 2010, **41**, 922–932.

13 C. Kuhnt, M. Karnahl, S. Tschierlei, K. Griebenow, M. Schmitt, B. Schafer, S. Krieck, H. Gorls, S. Rau, B. Dietzek and J. Popp, *Phys. Chem. Chem. Phys.*, 2010, **12**, 1357–1368.

14 K. Butsch, R. Gust, A. Klein, I. Ott and M. Romanski, *Dalton Trans.*, 2010, **39**, 4331–4340.

15 R. Horvath and K. C. Gordon, *Inorg. Chim. Acta*, 2011, **374**, 10–18.

16 A. E. Friedman, J.-C. Chambron, J.-P. Sauvage, N. J. Turro and J. K. Barton, *J. Am. Chem. Soc.*, 1990, **112**, 4960–4962.

17 M. K. Brennaman, T. J. Meyer and J. M. Papanikolas, *J. Phys. Chem. A*, 2004, **108**, 9938–9944.

18 B. Schafer, H. Gorls, M. Presselt, M. Schmitt, J. Popp, W. Henry, J. G. Vos and S. Rau, *Dalton Trans.*, 2006, 2225–2231.

19 M. K. Kuimova, W. Z. Alsindi, A. J. Blake, E. S. Davies, D. J. Lampus, P. Matousek, J. McMaster, A. W. Parker, M. Towrie, X.-Z. Sun, C. Wilson and M. W. George, *Inorg. Chem.*, 2008, **47**, 9857–9869.

20 H. van der Salm, M. G. Fraser, R. Horvath, S. A. Cameron, J. E. Barnsley, X.-Z. Sun, M. W. George and K. C. Gordon, *Inorg. Chem.*, 2014, **53**, 3126–3140.

21 H. E. Gottlieb, V. Kotlyar and A. Nudelman, *J. Org. Chem.*, 1997, **62**, 7512–7515.

22 S. L. Howell and K. C. Gordon, *J. Phys. Chem. A*, 2004, **108**, 2536–2544.

23 S. J. Lind, K. C. Gordon and M. R. Waterland, *J. Raman Spectrosc.*, 2008, **39**, 1556–1567.

24 S. J. Lind, T. J. Walsh, A. G. Blackman, M. I. J. Poulson, G. I. S. Irwin and K. C. Gordon, *J. Phys. Chem. A*, 2009, **15**, 3566–3575.

25 R. Horvath, M. G. Fraser, S. A. Cameron, A. G. Blackman, P. Wagner, D. L. Officer and K. C. Gordon, *Inorg. Chem.*, 2013, **52**, 1304–1317.

26 M. J. Frisch, G. W. Trucks, H. B. Schlegel, G. E. Scuseria, M. A. Robb, J. R. Cheeseman, G. Scalmani, V. Barone, B. Mennucci, G. A. Petersson, H. Nakatsuji, M. Caricato, X. Li, H. P. Hratchian, A. F. Izmaylov, J. Bloino, G. Zheng, J. L. Sonnenberg, M. Hada, M. Ehara, K. Toyota, R. Fukuda, J. Hasegawa, M. Ishida, T. Nakajima, Y. Honda, O. Kitao, H. Nakai, T. Vreven, J. J. A. Montgomery, J. E. Peralta, F. Ogliaro, M. Bearpark, J. J. Heyd, E. Brothers, K. N. Kudin, V. N. Staroverov, R. Kobayashi, J. Normand, K. Raghavachari, A. Rendell, J. C. Burant, S. S. Iyengar, J. Tomasi, M. Cossi, N. Rega, J. M. Millam, M. Klene, J. E. Knox, J. B. Cross, V. Bakken, C. Adamo, J. Jaramillo, R. Gomperts, R. E. Stratmann, O. Yazyev, A. J. Austin, R. Cammi, C. Pomelli, J. W. Ochterski, R. L. Martin, K. Morokuma, V. G. Zakrzewski, G. A. Voth, P. Salvador, J. J. Dannenberg, S. Dapprich, A. D. Daniels, O. Farkas, J. B. Foresman, J. V. Ortiz, J. Cioslowski and D. J. Fox, *Gaussian 09 Revision A.02*, 2009, Gaussian Inc., Wallingford CT.

27 D. M. Chipman, *J. Chem. Phys.*, 2000, **112**, 5558.

28 E. Cances, B. Mennucci and J. Tomasi, *J. Chem. Phys.*, 1997, **107**, 3032–3041.

29 M. Abrahamsson, M. J. Lundqvist, H. Wolpher, O. Johansson, L. Eriksson, J. Bergquist, T. Rasmussen, H.-C. Becker, L. Hammarström, P.-O. Norrby, B. Åkermark and P. Persson, *Inorg. Chem.*, 2008, **47**, 3540–3548.

30 M. G. Fraser, A. G. Blackman, G. I. S. Irwin, C. P. Easton and K. C. Gordon, *Inorg. Chem.*, 2010, **49**, 5180–5189.

31 R. Horvath and K. C. Gordon, *Coord. Chem. Rev.*, 2010, **254**, 2505–2518.

32 N. J. Lundin, P. J. Walsh, S. L. Howell, J. J. McGarvey, A. G. Blackman and K. C. Gordon, *Inorg. Chem.*, 2005, **44**, 3551–3560.

33 G. Schaftenaar and J. Noordik, *J. Comput. Aided Mol. Des.*, 2000, **14**, 123–134.

34 C. B. Larsen, H. van der Salm, C. A. Clark, A. B. S. Elliott, M. G. Fraser, R. Horvath, N. T. Lucas, X.-Z. Sun, M. W. George and K. C. Gordon, *Inorg. Chem.*, 2014, **53**, 1339–1354.

35 M. R. Waterland, K. C. Gordon, J. J. McGarvey and P. M. Jayaweera, *Dalton Trans.*, 1998, 609–616.

36 M. G. Fraser, H. van der Salm, S. A. Cameron, J. E. Barnsley and K. C. Gordon, *Polyhedron*, 2013, **52**, 623–633.

37 P. J. Walsh, K. C. Gordon, N. J. Lundin and A. G. Blackman, *J. Phys. Chem. A*, 2005, **109**, 5933–5942.

38 L. Tan, J. Shen, J. Liu, L. Zeng, L. Jin and C. Weng, *Dalton Trans.*, 2012, **41**, 4575–4587.

39 A. Arancibia, J. Concepcion, N. Daire, G. Leiva, A. M. Leiva, B. Loeb, R. D. Ro, R. Daz, A. Francois and M. Saldivia, *J. Coord. Chem.*, 2001, **54**, 323–336.

40 J. Dyer, W. J. Blau, C. G. Coates, C. M. Creely, J. D. Gavey, M. W. George, D. C. Grills, S. Hudson, J. M. Kelly, P. Matousek, J. J. McGarvey, J. McMaster, A. W. Parker, M. Towrie and J. A. Weinstein, *Photochem. Photobiol. Sci.*, 2003, **2**, 542–554.

41 M. Li, Z. Xu, X. You, X. Zheng and H. Wang, *Chem. Phys. Lett.*, 1998, **288**, 459–463.

42 L. A. Worl, R. Duesing, P. Chen, L. Della Ciana and T. J. Meyer, *Dalton*

Trans., 1991, 849–858.

43 C. Goze, C. Leiggener, S.-X. Liu, L. Sanguinet, E. Levillain, A. Hauser and S. Decurtins, *ChemPhysChem*, 2007, **8**, 1504–1512.

44 A. W. Adamson, *J. Chem. Educ.*, 1983, **60**, 797.

45 R. F. Dallinger and W. H. Woodruff, *J. Am. Chem. Soc.*, 1979, **101(15)**, 4391–4393.

46 P. G. Bradley, N. Kress, B. A. Hornberger, R. F. Dallinger and W. H. Woodruff, *J. Am. Chem. Soc.*, 1981, **103(25)**, 7441–7446.

47 J. V. Caspar, T. D. Westmoreland, G. H. Allen, P. G. Bradley, T. J. Meyer and W. H. Woodruff, *J. Am. Chem. Soc.*, 1984, **106(12)**, 3492–3500.

48 J. R. Schoonover, K. M. Omberg, J. A. Moss, S. Bernhard, V. J. Malueg, W. H. Woodruff and T. J. Meyer, *Inorg. Chem.*, 1998, **37(10)**, 2585–2587.

49 K. C. Gordon and J. J. McGarvey, *Chem. Phys. Lett.*, 1990, **173**, 443–448.

50 K. C. Gordon and J. J. McGarvey, *Inorg. Chem.*, 1991, **30**, 2986–9.